Peptide-functionalized nanoparticles for selective targeting of pancreatic tumor.

Peptide-functionalized Nanoparticles for Selective Targeting of Pancreatic Tumor

Sabrina Valetti [a,b], Federica Maione [c], Simona Mura [a], Barbara Stella [b], Didier Desmaële [a], Magali Noiray [a], Juliette Vergnaud [a], Christine Vauthier [a], Luigi Cattel [b], Enrico Giraudo [b,c], Patrick Couvreur [a]*

[a] Université Paris-Sud, Faculté de Pharmacie, 5 rue Jean-Baptiste Clément, 92296 Châtenay-Malabry cedex, France
CNRS UMR 8612, Institut Galien Paris-Sud, 5 rue Jean-Baptiste Clément, 92296 Châtenay-Malabry cedex, France
[b] Department of Science and Drug Technology, University of Torino, 9 via Pietro Giuria 10125 Torino, Italy
[c] Laboratory of Transgenic Mouse Models, Candiolo Cancer Institute – FPO, IRCCS, Strada Provinciale 142, Km. 3.95 10060 Candiolo (Torino), Italy

*To whom correspondence should be addressed.
E-mail: patrick.couvreur@u-psud.fr
Tel: +33 1 46 83 53 96
Fax: +33 1 46 83 55 11

Abstract

Chemotherapy for pancreatic cancer is hampered by the tumor physio-pathological complexity. Here we show a targeted nanomedicine using a new ligand, the CKAAKN peptide, which had been identified by phage display, as an efficient homing device within the pancreatic pathological microenvironment. Taking advantage of the squalenoylation platform, the CKAAKN peptide was conjugated to squalene (SQCKAAKN) and then co-nanoprecitated with the squalenoyl prodrug of gemcitabine (SQdFdC) giving near monodisperse nanoparticles (NPs) for safe intravenous injection. By interacting with a novel target pathway, the Wnt-2, the CKAAKN functionalization enabled nanoparticles: (i) to specifically interact with both tumor cells and angiogenic vessels and (ii) to simultaneously promote pericyte coverage, thus leading to the normalization of the vasculature likely improving the tumor accessibility for the therapy. **All together, this approach represents a unique targeted nanoparticle design with remarkable selectivity towards pancreatic cancer and multiple mechanism of action.**

Graphical abstract

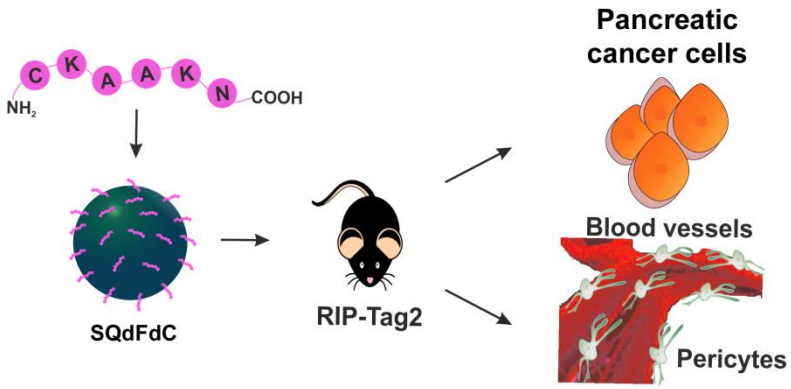

Keywords

Targeted nanoparticles; tumor-targeting peptide; squalene nanoparticles; pancreatic cancer; gemcitabine.

Introduction

Pancreatic cancer is a devastating disease which represents the fourth leading cause of cancer-related death in the European Community and in North America [1]. The median survival is less than 6 months and the maximum is 5 years for 6% of patients [2]. Despite this high mortality, pancreatic cancer represents only the 10^{th} most common cause of new cancers. This imbalance between frequency and mortality is because most patients are diagnosed at an unresectable, advanced and metastatic stage for which, at the moment, only palliative treatments are available, due to the lack of sensitivity of pancreatic cancer to many chemotherapeutic drugs [2]. Despite the decline over the past decade in the global mortality related to lung, colon, prostate and breast cancer, the progresses in pancreatic cancer therapy had remained exceedingly slow and disappointing without impairing the death rate. Since 1996, gemcitabine (dFdC), a nucleoside analogue that blocks DNA replication, has been the major chemotherapic agent for pancreatic cancer treatment [2]. Despite its weak response rate of 5% and the modest overall survival benefit, this drug still remains the first-line treatment in the clinical practice.

Several combined protocol therapies with gemcitabine have been tested in randomized clinical trials [3, 4]. Only erlotinib, an inhibitor of the epidermal growth factor receptor and recently (September 2013) Abraxane (paclitaxel albumin-bound nanoparticles) have been approved by the FDA in combination with gemcitabine due to the significant improvement in patient survival and delay in tumor growth [5-7]. Due to its rather hydrophilic character, gemcitabine is unable to passively diffuse across the plasma membrane but it is transported into the cell by either human equilibrative (hENT) or sodium-gradient nucleoside transporters. The resistance to gemcitabine treatment often arises from the down regulation of these nucleoside transporters which impairs gemcitabine membrane transport, as shown in both the pre-clinical experimental models and the clinic [8]. Gemcitabine is also rapidly inactivated into the blood, due to the fast metabolization by blood deaminases, into the inactive difluorouracil. Thus, a frequent administration schedule at a high drug dose (usually 800-1000 mg/m^2, 30 min infusion) is required. Additionally, the poor tumor tissue perfusion resulting from deprived vascularization, the formation of a dense stroma and the important heterogeneity of pancreatic cancer cells dramatically hamper drug efficacy and bioavailability in the tumor tissue, also leading to significant side effects [9].

Drug nanocarriers decorated with hydrophilic and flexible polymers, such as poly(ethylene glycol) (PEG), have been proposed to improve drug accumulation at the tumor target site through the so-called Enhanced Permeability and Retention (EPR) effect that takes advantage of the highly irregular tumor vasculature with abnormal heterogeneous density, the large pores on the endothelial walls and the reduced lymphatic drainage in tumor tissue [10, 11]. However in several tumors, such passive targeting is inefficient. Therefore, the development of targeted therapeutic approaches, using nanoparticles (NPs) able to specifically bind to receptors mainly expressed onto malignant cells and relatively down regulated in healthy ones [12], represents an attractive therapeutic alternative [13-15]. To date, there are very few examples of drug-loaded nanoparticles functionalized with specific ligands showing a therapeutic efficacy in experimental pancreatic cancer models. For instance, nanocarriers were decorated with the epidermal growth factor receptor (EGFR) [16], the arginine-glycine-aspartic acid (RGD) peptide [17] or an antibody towards the transferrin receptor [18]. However, apart from the fact that these nanodevices exhibited poor drug loading [17, 18] they were functionalized with homing devices not specific for pancreatic cancer since typically expressed also on several other types of healthy and/or cancer cells. This explains the inability

of these materials to reach the pancreatic cancer tissue, even at a low concentration [19].Therefore, the discovery of more specific ligands for pancreatic tumor targeting is urgently needed and represents an important challenge.

In this context, we have taken advantage of previous findings that, starting from a phage-displayed peptide library screening on mouse models of cancer, described peptides that selectively bind tumor vasculature [20]. The main advantage of this approach consists in the identification of novel peptide ligands, able to specifically interact with the target disease marker proteins, which are accessible *via* the systemic circulation within a definite pathological microenvironment. In particular Joyce *et al.* [20] identified a linear peptide composed by 6 aminoacids (*i.e.* CKAAKN) which specifically bound tumor vessels in the RIP-Tag2 transgenic mice, a prototypical mouse model of multistage pancreatic islet cell carcinoma [20, 21].

Motivated by this findings, we have constructed a novel efficient targeted nanomedicine for pancreatic cancer treatment, using squalene, a natural and biocompatible lipid as carrier material [21], gemcitabine as anticancer drug and the CKAAKN peptide as homing device. After chemical modification, the squalene was conjugated to either gemcitabine (SQdFdC) or to CKAAKN peptide (SQCKAAKN).

1. Materials and methods

1.1. Materials

1,1',2-Trisnor-squalenic aldehyde was obtained from squalene as previously described [21]. Gemcitabine hydrochloride (difluorodeoxycytidine (dFdC)) was purchased from Sequoia Research Products Ltd (UK). 4-(*N*)-trisnorsqualenoyl-gemcitabine (SQdFdC) was obtained as previously reported [22]. CKAAKN peptide was purchased from CASLO Laboratory Aps (Denmark). Squalene, dextrose and all other reagents were obtained by Sigma-Aldrich Chemical (Italy). All solvents were of analytical grade from Carlo Erba Reagenti (Italy) or VWR (France). The ^{1}H NMR and ^{13}C NMR spectra were recorded on Bruker Avance 300 (300 MHz, 75 MHz) or Bruker Avance 400 (400 MHz, 100 MHz) spectrometers in $CDCl_3$, CD_3COCD_3, CD_3OD or D_2O. Multiplicities of resonances are described as broad (b), singlet (s), doublet (d), triplet (t), or multiplet (m). Recognition of methyl, methylene, methine, and quaternary carbon nuclei in ^{13}C NMR spectra rests on the J-modulated spin-echo sequence. Mass spectra were obtained using electrospray ionization (ESI) conditions in a positive-ion or a negative-ion mode either on Finnigan-MAT TSQ 700 spectrometer (CA) or Esquire LC Bruker spectrometers. All reactions involving air- or water-sensitive compounds were routinely conducted in glassware which was flame-dried under a positive pressure of nitrogen. The reactions were monitored by thin-layer chromatography (TLC) on F254 silica gel pre-coated plates. After development, the plates were viewed under UV light (254 nm) and visualized with I_2 or Kägi-Misher reagents. Flash-column chromatography was performed on CombiFlash® Rf systems (Teledyne ISCO, Italy) on appropriate columns (silica or RP18). All solvents were distilled prior to flash chromatography.

1.2. Synthesis and characterization of 6-(maleimidyl)-hexanoic acid (trisnor-squalenylidene)-hydrazide (9)

A solution of 1,1',2-trisnor-squalenic aldehyde **(8)** (0.334 g, 0.868 mmol) in CH_2Cl_2 was added to dry methanol (15 mL). The resulting mixture was sonicated few minutes until complete dissolution. [6-(maleimido)hexanamido]azanium trifluoroacetate **(7)** [23] (0.306 g, 0.868 mmol) and 4 Å molecular sieves (200 mg) were then added and the reaction mixture was stirred for 1 h at room temperature under nitrogen. The formation of the desired product **(9)** was monitored by TLC (petroleum ether/ethyl acetate 1/1 v/v, R_f: 0.65). The mixture was filtered and concentrated under reduced pressure. The residue was taken into water (5 mL) and extracted with CH_2Cl_2 (3 x 15 mL). The combined organic phases were dried over anhydrous $MgSO_4$ and concentrated *in vacuo*. Purification by flash-chromatography on silica column, eluting with a gradient of petroleum ether to petroleum ether/ethyl acetate 60/40 v/v, gave the product as a light yellow waxy material (0.211 g, 63% yield) (Supplementary material, Figure S1).
^{1}H NMR ($CDCl_3$) δ: 8.39 (s, 1H, C*H*=NN), 7.05 (t, *J* = 5.2 Hz, 1H, N*H*CO), 6.68 (s, 2H, CO-C*H*=C*H*CO), 5.14-5.07 (m, 5H, *H*C=C(CH_3)), 3.54-3.49 (t, *J* = 7.2 Hz, 2H, CH_2N), 2.70-2.50 (m, 2H, CH_2CONH), 2.40-1.90 (m, 20H, =C(CH_3)CH_2CH_2), 1.80 (s, 3H, HC=C(CH_3)$_2$), 1.76-1.65 (m, 12H, HC=C(CH_3)CH_2), 1.62-1.60 (m, 4H, NCH_2CH_2CH_2CH_2CH_2CON), 1.41-1.33 (m, 2H, NCH_2CH_2CH_2CH_2CH_2CON). ^{13}C NMR ($CDCl_3$) δ: 171.2, 166.3, 147.3, 135.8, 135.7-132.0, 125.9-124.7, 42.5, 39.7-26.4, 38.2, 36.6, 31.0, 26.9, 25.9, 24.6-16.4, 22.4. MS (EI): *m/z(%)* 81 (70), 110 (100), 192 (55), 591 (3). HPLC analysis: Symmetry C18 column, 5 μm (Merck, Italy) equipped with a C18 column guard, elution with 100% methanol, detection by UV adsorption measurement at 237 nm (flow rate 1 mL/min, t_r=5.79 min). Peak heights were recorded and processed on a CBM-10A Shimadzu interface.

*1.3. Synthesis and characterization of the Michael adduct of CKAAKN and 6-(maleimidyl)-hexanoic acid (trisnor-squalenylidene)-hydrazide (SQ-CKAAKN, **(5)**)*

A mixture of **(9)** (13.5 mg, 0.0229 mmol) and CKAAKN peptide (**4**) (7.25 mg, 0.0114 mmol) in dimethylformamide DMF/H_2O 3/1 v/v (2 mL) was stirred for 3 h at 40 °C. The reaction mixture was then concentrated under reduced pressure and the crude product was taken into diethyl ether to remove unreacted maleimide. The supernatant was withdrawn after decantation (3 times). In order to eliminate unreacted peptide, the solid was dissolved in methanol and filtered through a sintered glass funnel. The product was obtained as a translucent waxy material (10 mg, 0.0082 mmol, 70% yield); MS (+ESI): *m/z* (%) = 1226.0 (100) $[MH]^+$, 614.5 (2) (Fig.1).

1.4. Preparation of nanoparticles

SQdFdC and SQdFdC/SQCKAAKN nanoparticles were prepared by the nanoprecipitation technique [24]. Practically, for SQdFdC NPs, SQdFdC was dissolved in ethanol (40 mg/mL) and then added dropwise under magnetic stirring into 1 mL of MilliQ® water (ethanol/water 0.1/1 v/v). Formation of the nanoparticles occurred spontaneously without using any surfactant. After solvent evaporation under reduced pressure, an aqueous suspension of pure SQdFdC nanoparticles was obtained (final SQdFdC concentration 4 mg/mL). For SQdFdC/SQCKAAKN NPs the two compounds were dissolved in 0.1 mL of ethanol at 1:0.01 SQdFdC/SQCKAAKN molar ratio. The organic solution was then added dropwise under magnetic stirring into 1 mL of MilliQ® water (ethanol/water 0.1/1 v/v). After solvent

evaporation under reduced pressure, an aqueous suspension of SQdFdC/SQCKAAKN NPs was obtained (final SQdFdC concentration: 3.4 mg/mL).

Fluorescent nanoparticles were obtained using the same procedure, unless 1% (w/w), of the fluorescent probe CholEsteryl BODIPY® FL C12 (BChol-green, Life Technologies, Molecular Probes, France) was dissolved in the ethanolic solution before dropwise addition into water. Ethanol was evaporated as described above. All the formulations were stored at room temperature.

1.5. Nanoparticle characterization

The mean particle size and polydispersity index of SQdFdC NPs and of SQdFdC/SQCKAAKN NPs were measured by dynamic light scattering (DLS) with a Nano ZS from Malvern (UK) (173° scattering angle) at 25 °C. The measurements were performed after dilution of the NPs suspensions 1:25 in MilliQ® water. The NPs surface charge was investigated by zeta potential measurements at 25°C after dilution with 0.05 mM KCl solution, applying the Smoluchowski equation and using the same apparatus. Measurements were carried out in triplicate. The colloidal stability was investigated by measuring the nanoparticle mean diameter over a period of 72 hours (Supplementary material, Figure S2). The morphology of the nanoparticles was examined by cryogenic transmission electron microscopy (cryoTEM). Briefly, one drop (5 µL) of the nanoparticles suspensions (5 mg/mL) was deposited on a 200-mesh electron microscopy grid. Most of the drop was removed with a blotting filter paper and the residual thin film remaining within the holes was vitrified by plunging it into liquid ethane. The specimen was then transferred using liquid nitrogen to a cryo-specimen holder and observed using a JEOL 2100HC microscope.

1.6. Surface plasmon resonance analysis

Interaction analyses were performed on a BIAcore T100 instrument including CM5 Series S sensor chip (GE Healthcare Life Sciences Europe, France). All experiments were carried out at 25 °C in Dulbecco-PBS (D-PBS) running buffer. The immobilization process was performed with 150 mM phosphate buffer, pH 7.4 at a flow rate of 10 µL/min. The carboxymethylated dextran matrix was activated for 7 min with a mixture 1:1 *N*-ethyl-*N*'-(3-diethylaminopropyl)-carbodiimide (EDC) 0.1 M/ *N*-hydroxysuccinimide (NHS) 0.4M (GE Healthcare Life Sciences Europe, France). The sFRP-4 receptor was then injected over the activated surface at 10 µg/mL in 10 mM sodium acetate buffer at pH 4.4 during 7 min, giving an average immobilization level of 2800 resonance units (RU). Unreacted sites of the matrix were finally blocked by a 7-min injection of 1 M ethanolamine hydrochloride at pH 8.5. For reference, an additional blank flow channel was prepared according to the same process without injecting the receptor over the surface. Binding capacities of the functional surfaces were tested with 180 s injections of CKAAKN peptide solution, nanoparticles or nanoparticles functionalized with the CKAAKN peptide at different concentrations. All experiments were carried out in duplicate on the IPSIT platform (Châtenay-Malabry, France).

1.7. Evaluation of the activation of C3 protein of the complement system

The activation of the complement system (highlighted by the conversion of plasmatic C3 protein into C3b and C3a fragments) induced by the different nanoparticles was evaluated by 2-D immunoelectrophoresis using a polyclonal antibody to human C3 [25]. Human serum was obtained after calcifying plasma from healthy donors (EFS Ile-de-France, France) and stored at −80 °C until use. Veronal-buffered saline (VBS) containing 0.15 mM Ca^{2+} and 0.5 mM

Mg^{2+} ions (VBS^{2+}) and VBS containing 40 mM ethylenediaminetetraacetic acid (VBS–EDTA) were prepared as described by Kazatchkine *et al.* [26] Complement C3 antiserum rose in goat was purchased from Sigma-Aldrich (France). To ensure a valid comparison of the different nanoparticles, each sample was concentrated up to 6 mg/mL to obtain a sufficient specific surface (S_{specif} = 6 m/Dd, where m is the mass contained in the sample, D is the average diameter and d is the density). 100 µL of nanoparticles (corresponding to an equivalent surface area of 167 cm^2) were incubated under gentle agitation for 1 h at 37 °C with 50 µL of human serum and 50 µL of VBS^{2+}. 100 µL of water were used as a control of spontaneous activation of C3 protein and 100 µL of redox radical emulsion polymerization (RREP) dextran (0.5%)-coated poly(isobutylcyanoacrylate) (PIBCA) nanoparticles [27] were used as positive control (Supplementary material, Figure S3). All experiments were performed with the same human serum whose functionality was tested before use (Supplementary material, Figure S3). After incubation, 7 µL of each sample were subjected to a first electrophoresis (600 V, 16 mA, 100 W, 70 min) on 1% agarose gel in tricine buffer, then the 2-D electrophoresis (500 V, 12 mA, 100 W, 18 h) was carried out on Gelbond® film coated with agarose gel containing a polyclonal antibody to human C3 at 0.1 mg/mL for detection of native and activated form of C3. Films were fixed in 0.15 M NaCl, further dried and stained with Coomassie blue to reveal the presence of native C3, and lower molecular weight activated fragments C3a and C3b precipitated with the antibody. Activation of the C3 protein was expressed as the complement activation factor (CAF) defined as the ratio of the peak surface of C3a+C3b detected on the plate over the sum of the peak surface of C3 and C3a+b. For the nanoparticles, the CAF was then normalized (CAF_n) on a scale ranging from 0 to 100 in which 100 indicated total activation and 0 the spontaneous activation measured in absence of nanoparticles. Areas under the peaks were measured using ImageJ® software. All experiments were set up in triplicate or more to determine means and SD.

1.8. Transgenic tumor model

The RIP-Tag2 transgenic mouse model has been previously reported [28]. Transgenic mice were generated by backcrossing transgenic males with C57Bl/6 females (Jackson Laboratory, USA). All animal procedures were approved by the Ethical Commission of the University of Turin and by the Italian Ministry of Health in compliance with the international laws and policies.

1.9. In vivo therapeutic efficacy

Tumor-bearing RIP-Tag2 mice were treated for two weeks, starting from 12 until 14 weeks of age. Mice were randomized and assigned to 4 groups of 8 mice each and all groups received four intravenous injections in the lateral tail vein on days 0, 3, 7 and 11 with either (i) 15 mg/kg dFdC; (ii) SQdFdC NPs at dFdC equivalent dose of 15 mg/kg; (iii) SQdFdC/SQCKAAKN NPs at dFdC equivalent dose of 15 mg/kg or (iv) saline control solution. In order to obtain an isosmotic solution, dextrose (5% w/w) was added to the nanoparticle suspensions and their colloidal stability was investigated by measuring mean diameter (Supplementary material, Figure S2). Mice were monitored regularly for changes in weight and health status. Mice were humanely sacrificed on day 12. A pre-treatment with 5mg/kg of dexamethasone (Decadron®, CABER S.p.A., Italy) was performed by intramuscular injection 4 h before the treatment. No toxicity of nanoparticles or gemcitabine was observed at the dose tested.

1.10. Tissue preparation and histology

Tumor tissues were fresh frozen in Optimum Cutting Temperature (O.C.T. Tissue Tek) and cut in 10 µm thick sections using a Leica CM1900 cryostat. Sections were air-dried, fixed in zinc fixative (6.05 g Tris, 0.35 g Ca $(C_2H_3O_2)_2$, 2.5 g Zn $(C_2H_3O_2)_2$, 2.5 g ZnCl, 3.8 mL HCl 37%) for 10 min and they were blocked with 1% bovine serum albumin and 5% serum (donkey serum) in PBS. Tissues were then subjected to immunostaining with the following appropriate primary antibodies: purified rat monoclonal anti-Panendothelial cell antigen (Meca32) (clone Meca32, BD Pharmingen, USA), diluted 1/100; rabbit polyclonal anti-α-SMA (Abcam, UK), diluted 1/100**; rabbit anti-NG2 (Chondroitin sulphate proteoglycan polyclonal) (AB5320, Chemicon),** diluted 1:100 rabbit monoclonal anti-cleaved caspase-3 [29] (asp175, clone 5A1, Cell Signaling, USA), diluted 1/50 or rabbit polyclonal anti-Frizzled 5 (Abcam, UK) diluted 1/100. The secondary antibodies used were: anti-rabbit Alexa Fluor®488 or Alexa Fluor®555 and anti-rat Alexa Fluor®488 or Alexa Fluor®555 (1/400, Molecular Probes, USA). Nuclei were counterstained with DAPI (Invitrogen, USA). All immunofluorescence images were captured by using a Leica TCS SP2 AOBS confocal laser-scanning microscope (Leica Microsystems) maintaining the same laser power, gain and offset settings. All immune-localization experiments were performed on multiple tissue sections and included negative controls for determination of background staining, which was negligible.

1.11. In vivo NPs binding

A cohort of tumor-bearing RIP-Tag2 mice was pretreated with 5mg/kg Decadron for 4 hours and then alternatively injected with fluorescent SQdFdC NPs or SQdFdC/SQCKAAKN NPs. Free CholEsteryl BODIPY® FL C12 dye was used as negative control. Mice were sacrificed 6 hours after administration and tissues were collected and included freshly in OCT. Vessels were stained with Meca32 antibody and nuclei were counterstained with DAPI (as described in 1.10.Tissue preparation and histology). Confocal images were scored for the presence of fluorescent SQdFdC NPs or SQdFdC/SQCKAAKN NPs in the tumor context.

1.12. Ex vivo targeting and Flow cytometry analysis

A pool of purified pancreatic insulinomas was obtained from two end-stage RIP-Tag2 mice. Tissues were mechanically portioned through a McIlwain Tissue Chopper, resuspended in serum free L-15 Leibovitz medium (Sigma Aldrich) with 0.25mg collagenases B and D (Roche) and incubated for 10 minutes at 37°C under shaking. In order to isolate single cells, tissues were further digested in trypsin (Sigma Aldrich) and filtered with 70 µm cell strainer (BD Falcon). Samples were resuspended in MACS buffer (PBS pH 7.2, FCS 1%, 2mM EDTA) and incubated with 1 µM fluorescently labeled SQdFdC NPs, SQdFdC/SQCKAAKN NPs or free CholEsteryl BODIPY® FL C12 dye as negative control for 4 hours at 37°C in the dark. After washing with 1x PBS, tumor endothelial cells were stained for cytometry by anti-CD31-APC antibody (BD Pharmingen), in the dark at 4°C for 30 minutes. Then, samples were washed, resuspended in MACS buffer and analyzed on a flow cytometer (CyAn ADP, DakoCytomation).

1.13. Confocal microscopy quantifications

Quantifications of tumor vasculature were performed with MacBiophotonics ImageJ. The total area occupied by vessels was quantified as percentage of Meca32 positive staining on the tumor tissue area. For each animal, the total vessel area of 5 fields/mouse was quantified. To

quantify pericyte coverage (α-SMA, red channel) in each image, a region of interest (ROI) close to each blood vessel (Meca32, green channel) was drawn and then the mean fluorescence intensity (MFI) of red and green channels was quantified using the Leica Confocal Software Histogram Quantification Tool. The ratio between red and green channel MFI was then calculated; values were expressed as percentage of red-green co-staining. To determine the expression levels of caspase-3 (red channel) the number of cleaved caspase-3 positive cells on the total number of cells present in the tissue area was measured in each analyzed image.

1.14. Immunohistochemistry analysis

Frozen tumor sections were processed as previously described in the above "Tissue preparation and histology" section. Then, slides were permeabilized in 0.1% PBS, treated for 30 min with 3% hydrogen peroxide (Sigma-Aldrich, Italy) to quench endogenous peroxidases and saturated with protein block serum-free (Dako, Denmark). Tissues were stained with the rabbit polyclonal anti-Ki67 (Abcam, UK) primary antibody, diluted 1/100. Anti-rabbit horse radish-peroxydase-conjugate secondary antibody (EnVision; DakoCytomation, Denmark) was used, and the reaction was visualized with the AEC kit (DakoCytomation). Tissues were counterstained with Mayer hematoxylin (Vector Laboratories), mounted on glass slides, and visualized with a BX-60 microscope (Olympus) equipped with a color Qicam Fast 1394-digital CCD camera (12 bit; QImaging). The number of proliferating cells was evaluated by using ImageJ and considering 5 different fields/mouse. Values are presented as percent of Ki67 positive cells on total cell number.

1.15. Statistical analysis

The results of all experiments are expressed as mean ± SD. Statistical analyses were performed using a 2-tailed, unpaired Mann-Whitney U test. A *p* value below 0.05 was considered significant.

2. Results and discussion

2.1. Design and characterization of CKAAKN-functionalized nanoparticles

SQdFdC **(3)** was synthesized as reported elsewhere [22] by acylation of the C-4 nitrogen atom of the cytosine nucleus with 1,1',2- trisnor-squalenic acid **(2)** prepared from squalene (Fig. 1).

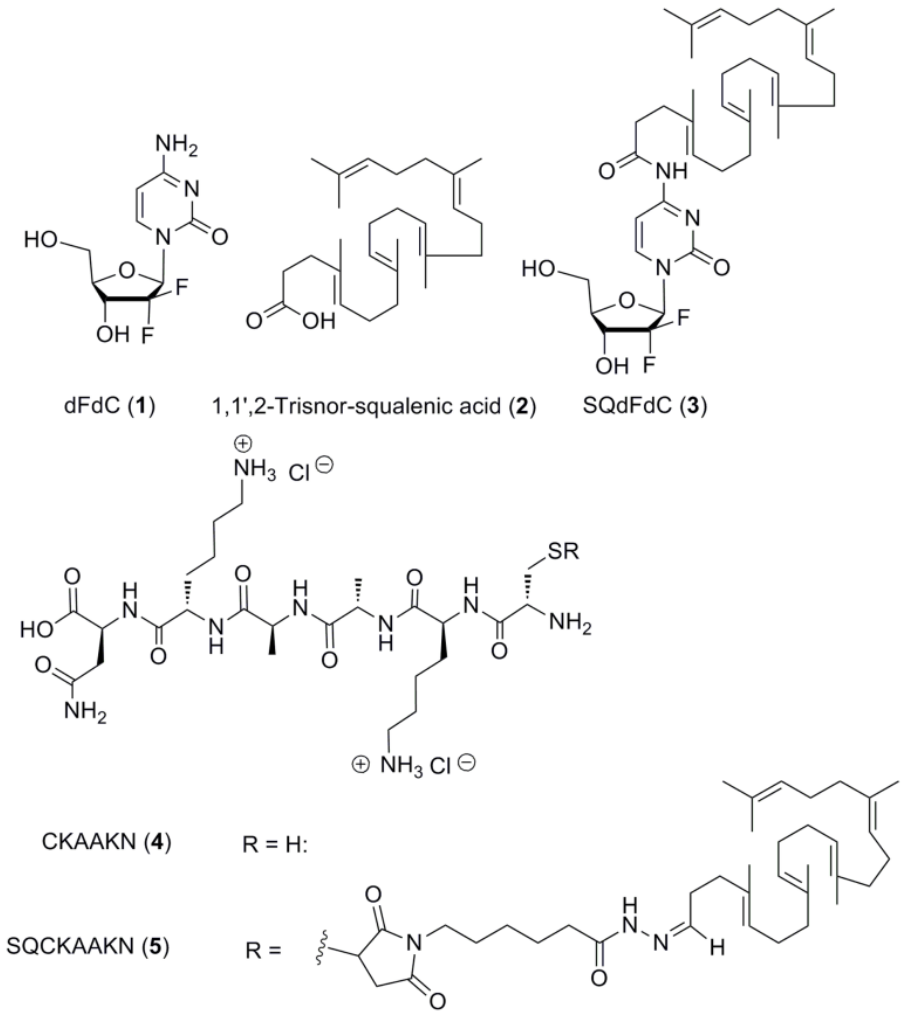

Fig. 1. Squalenoyl derivatives.

The obtained amphiphilic bioconjugate is able to spontaneously self-assemble in water into nanoparticles [22]. The thiol group of the N-terminal cysteine of the CKAAKN peptide **(4)** enabled the conjugation of the peptide to squalene, previously modified by the introduction of a 6 carbon atom lipophilic chain with a maleimide terminal group, which allowed to establish a hydrolysable bond between the squalene moiety and the maleimide group and a relatively stable thioether bond between the maleimide group and the peptide **(5)**. In spite of the difficulty to allow the highly hydrophilic peptide to react with the lipophilic squalene derivative, the thiol-maleimide Michael-type addition allowed to obtain the desired conjugate with a satisfactory 70% yield (Supplementary material, Figure S1). Thanks to their similar squalenoyl moiety, the simple addition of an ethanolic solution of the two materials (that is, SQdFdC/SQCKAAKN in 1/0.01 molar ratio) to water led to the spontaneous formation of nanoparticles without requiring any surfactant (ethanol/water 0.1/1 v/v). The obtained nanoparticle suspension was characterized by a high drug loading (~ 40%) and a narrow size distribution (average diameter of 130-170 nm with polydispersity index of 0.1) as confirmed by DLS and cryo-transmission electron microscopy (Fig. 2a,c).
Interestingly, the higher zeta potential value of SQdFdC/SQCKAAKN NPs, as compared with SQdFdC NPs (ZP average of -6 mV *vs* -22 mV), probably relies to the protonation of the lysine amino groups present in the CKAAKN structure, suggesting the presence of the peptide

onto the nanoparticle surface which is a crucial aspect to obtain an efficient cancer cell targeting.

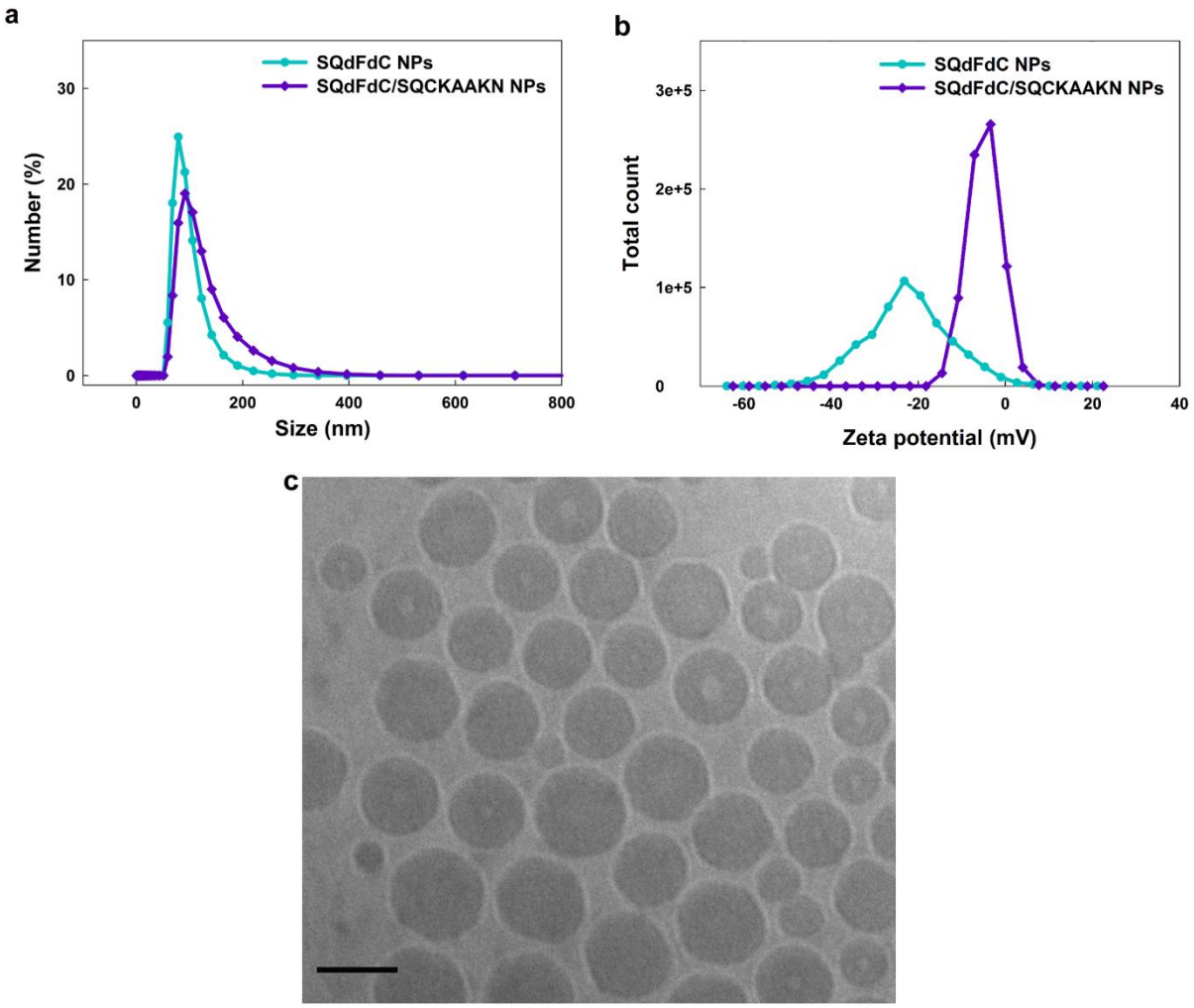

Fig. 2. Characterization of SQdFdC and SQdFdC/SQCKAAKN NPs.

2.2. Ligand-receptor interaction

In order to further confirm the surface localization of the CKAAKN peptide and to evaluate its targeting ability, the ligand-receptor binding of the peptide was investigated. Since it was reported by Joyce *et al* [20], that the sequence CKA-K shared motifs with the Wnt-2 protein, we tested if CKAAKN could act as Wnt-2 mimetic interacting with the Frizzled (FZD) receptors, by surface plasmon resonance (SPR). Among the FZD family, we focused our attention on the FZD-5 because it has been correlated with the development of vascular abnormalities and angiogenesis processes [30, 31].Since the receptor immobilization on the SPR biosensor could alter its conformation affecting the ligand binding, we chose to use the sFRP-4, a secreted frizzled-related protein with high FZD-5 sequence alignment (BLAST analysis) that was already successfully used to this aim keeping its recognition ability [32].
Interestingly, the CKAAKN peptide was able to specifically interact with the sensorchip-immobilized sFRP-4 confirming the correlation indicated previously (Supplementary

material, Figure S4) [20]. Remarkably, a more important plasmonic signal was obtained with SQdFdC/SQCKAAKN NPs, whereas no signal was observed under identical experimental conditions with non-functionalized SQdFdC NPs (Fig. 3).

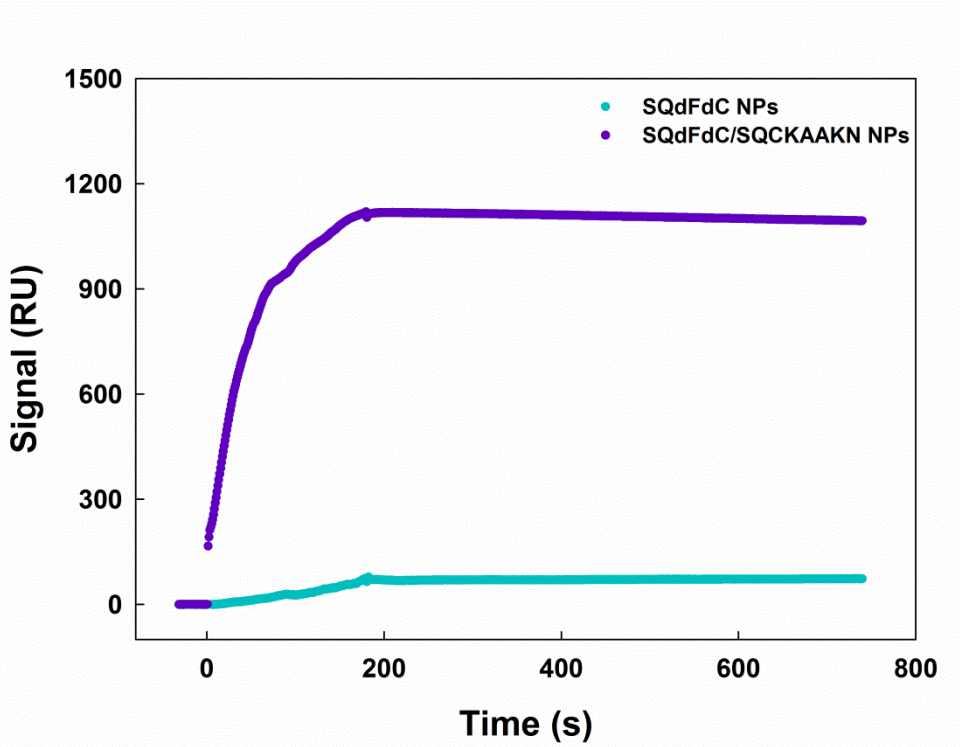

Fig. 3. Surface plasmon resonance analysis of SQdFdC NPs and SQdFdC/SQCKAAKN NPs.

Moreover, SQdFdC/SQCKAAKN NPs showed a concentration-dependent sensorgram profile (Supplementary material, Figure S5). The more important ligand-receptor interaction observed with CKAAKN-functionalized nanoparticles, as compared with the free peptide, demonstrated that the affinity of phage-display-derivated peptides can be significantly enhanced thanks to the multivalent interactions offered by a scaffold-like nanosized material in concordance with previous observations [33, 34]. Although peptides present several advantages in comparison to other targeting homing devices (*i.e.*, easy of synthesis and low immunogenicity), they usually possess modest target affinity. However, the conjugation of multiple copies of targeting ligand onto the nanocarrier surface, allows overcoming this limitation by enabling multivalent interaction with high binding constants and improving targeting efficacy [33]. These results allowed identifying the biological target of the CKAAKN peptide confirming also its surface localization.

The Wnt-2 belongs to a family of secreted lipid-modified signaling glycoproteins principally involved in embryonic development and tissue homeostasis [35]. Wnt-signaling pathway has also been shown to regulate the pancreatic β-cell endocrine function [36], proliferation, migration and differentiation [30]. Comprehensive genetic analysis [37-39] revealed that the Wnt is one of the six signaling pathways always altered in pancreatic cancers. [40] Its overexpression has recently been correlated to tumorigenesis, driving the self-renewal and differentiation of cancer stem cells and promoting the angiogenesis process [12, 35, 39, 41, 42]. On the basis of these observations, CKAAKN peptide, a specific Wnt-2 mimetic, may be

considered as a novel promising homing device to tailor targeted nanoparticle towards pancreatic cancer cells.

2.3. Complement activation in human serum

Taken together, these results clearly demonstrated the potential of CKAAKN-functionalized squalene-based nanoparticles to specifically interact with the target receptor. However, it has been reported that a high ligand density at the nanoparticle surface may promote idiosyncratic reactions based on complement activation and lead to a pseudo-allergic reaction (CARPA effect), which is responsible for thrombocytopenia, cardiopulmonary and hemodynamic changes that could conduce to death [43-45]. Therefore, SQdFdC/SQCKAAKN NPs and SQdFdC NPs were investigated for their ability of activating the complement C3 component, a key player in the activation of complement system [46]. It was observed that both types of NPs were very weak activators of the complement C3 component in human serum. Non-functionalized and CKAAKN-functionalized nanoparticles displayed, indeed, normalized Complement Activating Factor (CAFn) values of 10 ± 2.1% and 10 ± 2.8%, respectively (Fig. 4). **According to the literature [27, 47], SQdFdC NPs and SQdFdC/SQCKAAKN NPs displayed low capacity to activate the complement system thus supplementing the hypothesis of a safe intravenous administration.**

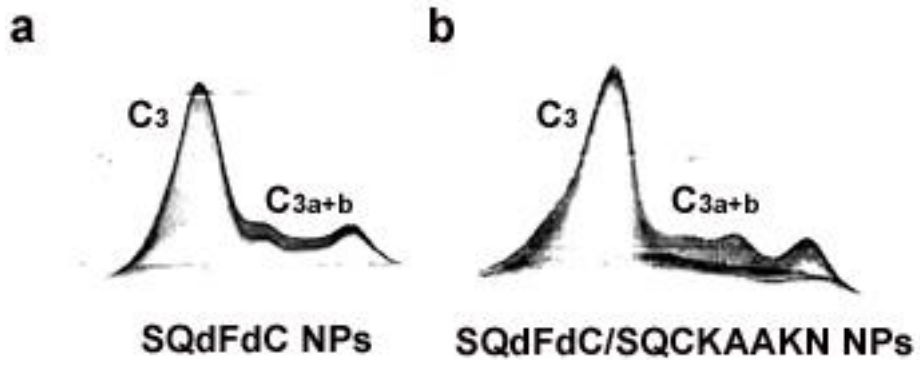

Fig. 4. Activation of C3 protein of the complement system.

2.4. Antitumor efficacy of CKAAKN-functionalized NPs in RIP-Tag2 mice

In the light of these results, we performed a regression trial to assess if SQdFdC/SQCKAAKN NPs were more efficient than SQdFdC NPs or dFdC in blocking tumor growth and angiogenic process in RIP-Tag2 mice, which were previously used for the phage-display screening [20]. RIP-Tag2 mice offer the advantage of both a spontaneous tumor development through multistage tumorigenesis and a well-documented angiogenic switching, in parallel to cancer progression. This well-characterized mouse model represents a suitable and highly reproducible platform to perform pre-clinical trials to test the effects of and anti-tumor and anti-angiogenic drug [28, 48-52]. In this work we used RIP-Tag2 mice as

proof-of-concept model to assess the ability of SQdFdC/SQCKAAKN NPs to impair tumor angiogenesis and, at the same time, to regress the growth of established cancers, Twelve week-old tumor-bearing RIP-Tag2 mice were injected intravenously (days 0, 3, 7 and 11) with either dFdC (15 mg/kg), SQdFdC NPs (15 mg/kg eq. dFdC) or SQdFdC/SQCKAAKN NPs (15 mg/kg eq. dFdC) and compared with saline-treated control mice. All treatments induced a significant reduction of the tumor volume compared with saline treated controls. SQdFdC NPs reduced tumor burden by 32% compared with dFdC, confirming the superior activity of squalenoyl gemcitabine nanoparticles, already demonstrated in other animal tumor models [53-55]. Interestingly, SQdFdC/SQCKAAKN NPs displayed a greater efficacy in impairing tumor growth compared with SQdFdC NPs (by 40%) and with dFdC (by 60 %) (Fig. 5a).

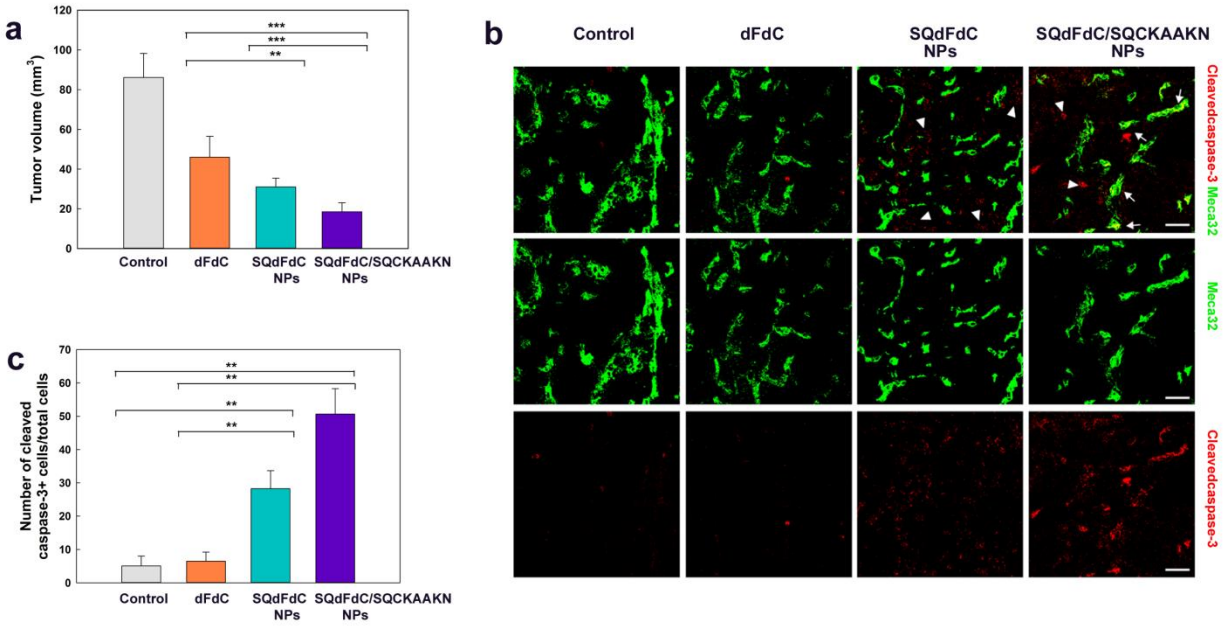

Fig. 5. Anti-tumor activity and apoptotic index.

The mechanism underlying the observed anticancer activity of CKAAKN-functionalized NPs was further investigated by assessing the proliferation and apoptosis indexes. Despite the fact that a significant reduction of cancer cell proliferation (anti-Ki67 Ab immune-staining) was observed in all treated groups compared with control (Supplementary material, Figure S6), the apoptotic rate (*i.e.*, anti activated caspase-3 immune-staining) was specifically increased in both nanoparticles-treated groups compared with dFdC and saline-treated ones (Fig. 5b,c). Treatment with NPs increased the apoptotic cell number in tumors by 82% compared with both dFdC and control groups. Remarkably, the treatment with SQdFdC/SQCKAAKN NPs induced a statistically significant increase (by 44%) in active caspase-3 immunostaining, compared with their non functionalized counterpart (Fig. 5c). Noteworthy is that the dramatic increase of apoptosis observed in SQdFdC/SQCKAAKN NPs group was detected not only in cancer cells but also in the tumor blood vessels (Fig. 5b). To better analyze the potential anti-angiogenic effect, we further analyzed the tumor vasculature and, by immunostaining with Meca-32 antibody and confocal analysis, we observed that SQdFdC/SQCKAAKN NPs dramatically reduced the vessel area by 58%, 55% and 57% compared with control, dFdC and

non functionalized NPs, respectively (Fig. 6a,b). Next we checked pericytes coverage of tumor blood vessels. **The quantification of α-smooth muscle actin (α-SMA) (Supplementary material, Figure S7) and NG2 co-localized with tumor endothelial cells revealed a greater pericyte coverage in SQdFdC/SQCKAAKN NPs-treated animals comparatively with SQdFdC NPs, dFdC and saline treated ones (by 40%, 39% and 39%, respectively) (Fig. 6c,d).** Increased pericyte coverage and reduction in vascular density are hallmarks of tumor blood vessel normalization. It has been proposed that the duration of the vascular normalization window, that allows more efficient delivery of oxygen and chemotherapeutic drugs into the tumor tissue, is critical to achieve a long-lasting and successful therapeutic synergy between antiangiogenic and chemotherapeutic drugs [50, 56]. **Taken together, these results suggest that the tumor regression observed with CKAAKN-functionalized nanoparticles resulted from a dual activity on both cancer cells and tumor vasculature. To consolidate this hypothesis, the tissues of tumor-bearing RIP-Tag2 mice were recovered upon injection of fluorescently-labeled NPs. A significant increase of SQdFdC/SQCKAAKN NPs accumulation in both tumor vasculature and cancer cells was observed compared with both non-functionalized NPs and the control (*i.e.*, the free fluorophore) (Figure 7). In addition, FACS analysis of fresh RIP-Tag2 tumors incubated with fluorescently-labeled NPs further confirmed the strong binding of peptide-functionalized NPs to tumor vasculature (tumor vessel/NPs 36% co-staining), compared to non-functionalized NPs (tumor vessel/NPs 10% co-staining) (Supplementary material, Figure S8).**

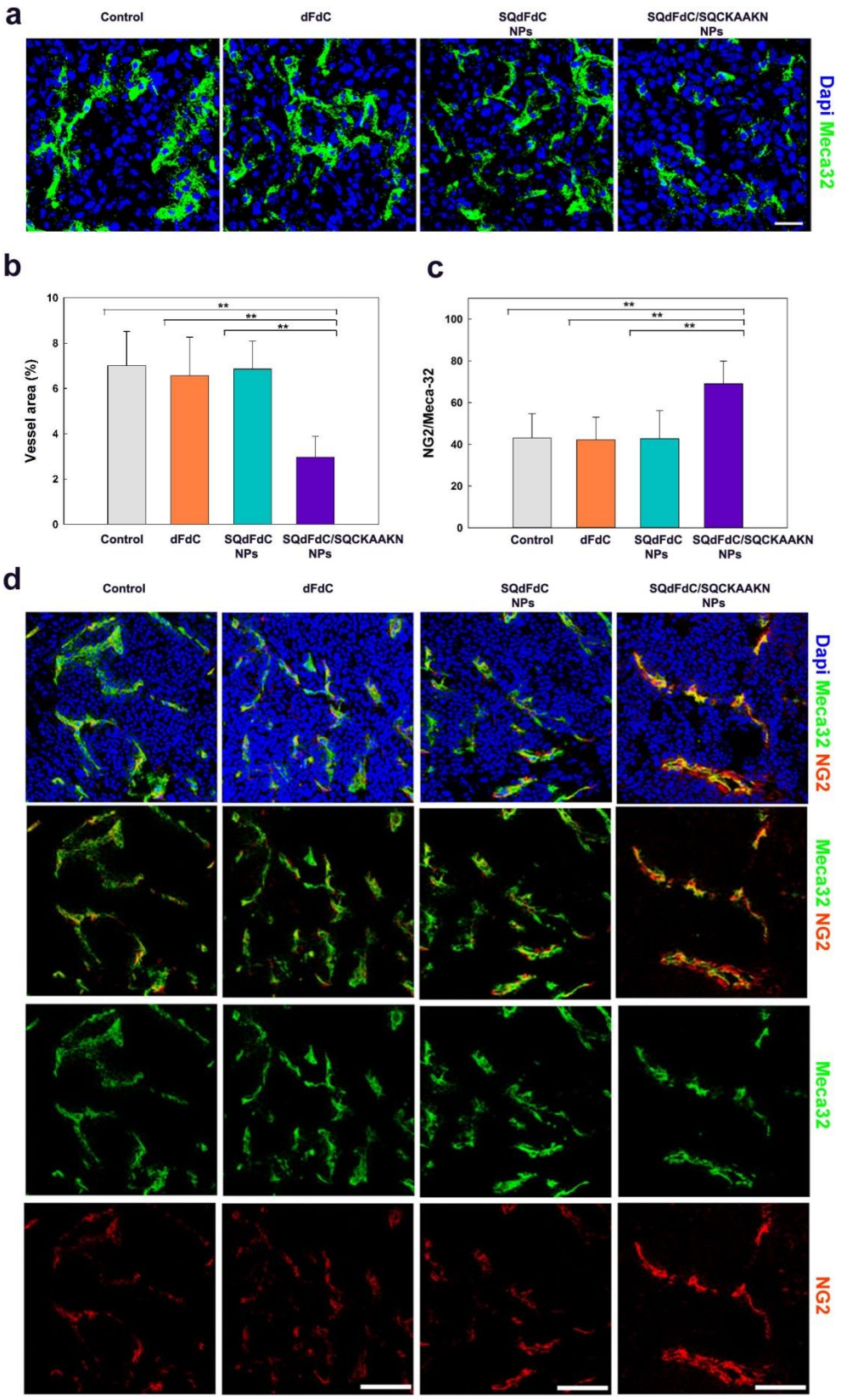

Fig. 6. Immunohistochemical staining of tumor tissue-vessels and pericyte quantification.

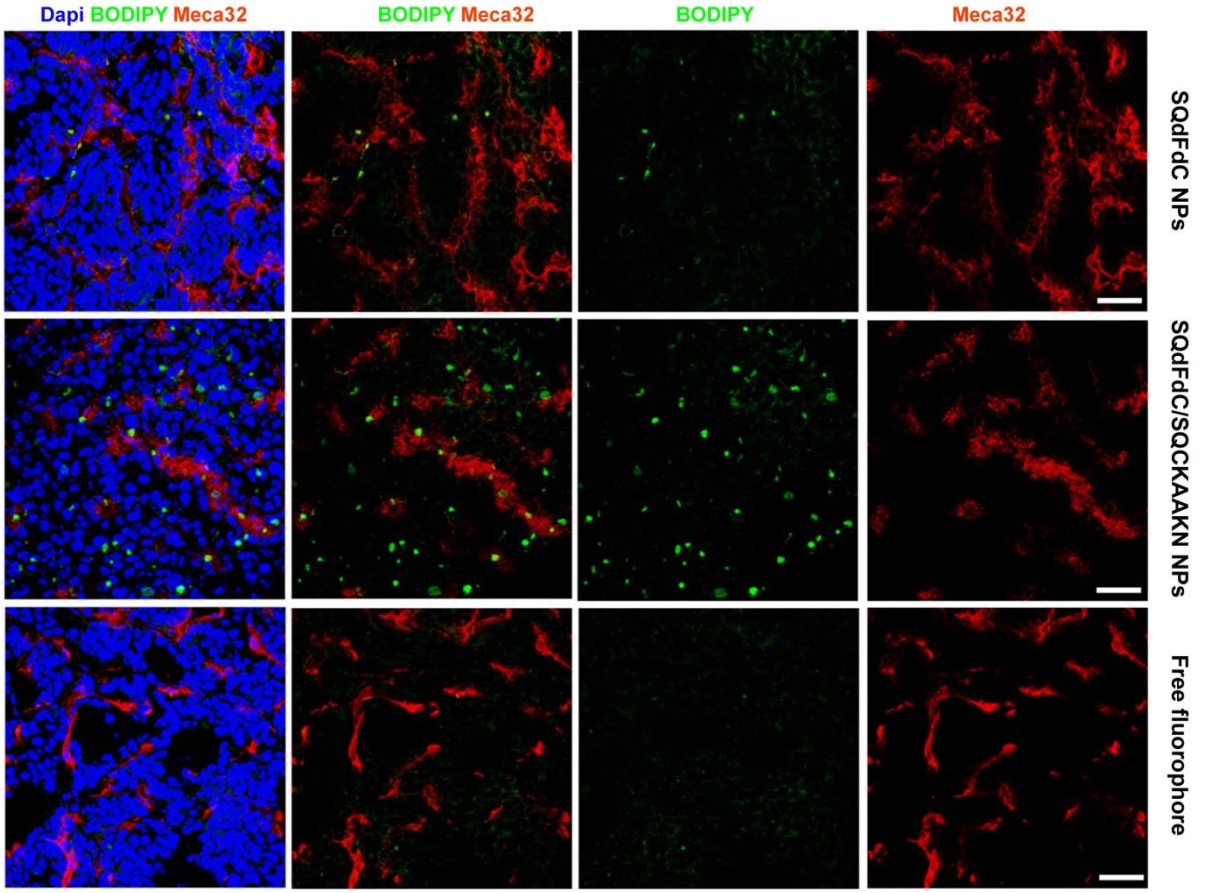

Fig. 7. Immunohistochemical staining of *in vivo* tumor tissue-vessels targeting by SQdFdC/SQCKAAKN NPs and SQdFdC NPs.

On the basis of previous data indicating the Wnt sharing motifs with the CKAAKN peptide [20] and of our data showing the FZD-5 as putative receptor for CKAAKN peptide-functionalized nanoparticles, we investigated the expression of FZD-5 in RIP-Tag2 tumors. Interestingly, we observed by immunostaining a strong expression of FZD-5 in tumor vasculature but also, although to a lower extent, in cancer cells of end-stage Rip-Tag2 tumors (Fig. 8).

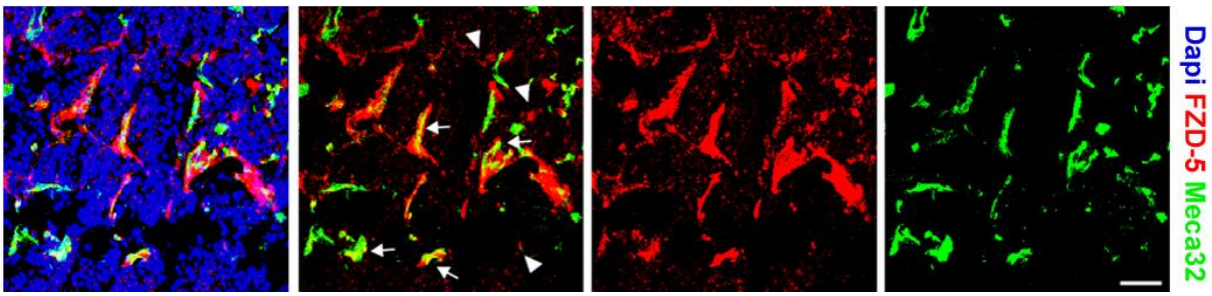

Fig. 8. Immunocytochemistry analysis and FZD-5 expression in tumor tissue.

These results pointed out that the enhanced antitumor activity observed for the CKAAKN-functionalized squalene-gemcitabine nanoparticles reflects by the multiple ability of (i) targeting both tumor and vessel cells, (ii) inhibiting tumor growth and angiogenesis and (iii) normalizing the vasculature [51, 52] (Fig. 9).

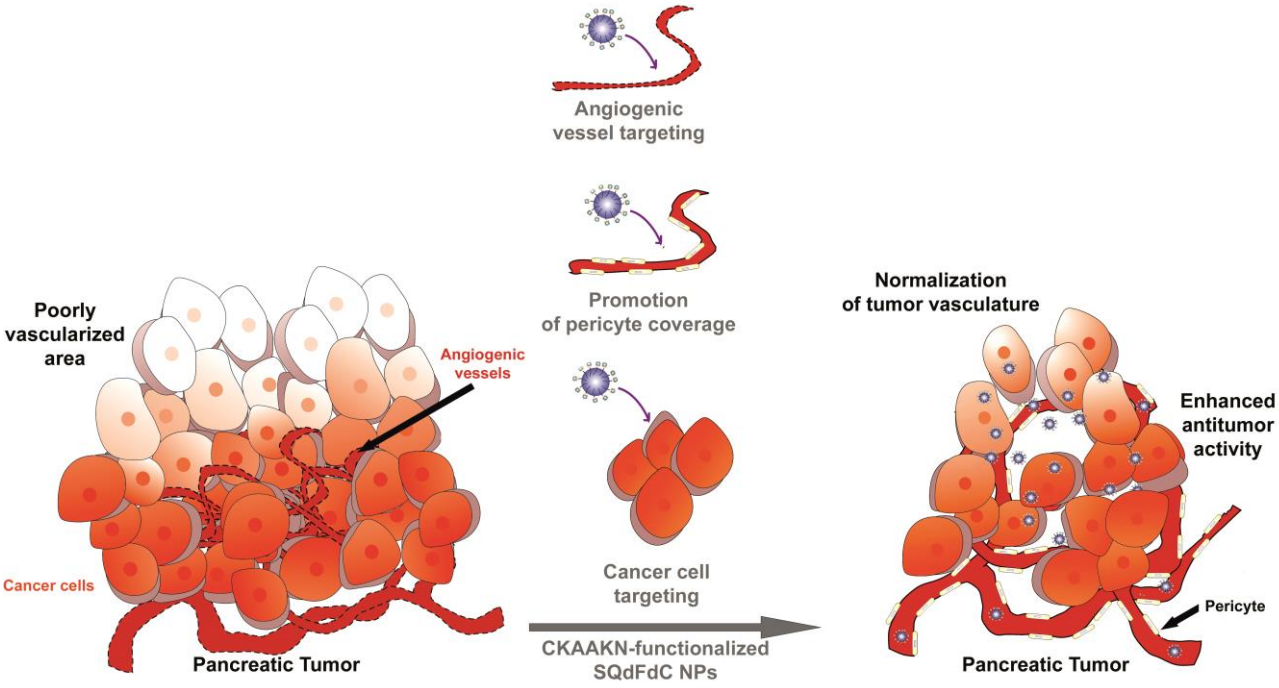

Fig. 9. Schematic representation of the selective targeting of pancreatic tumor and multiple mechanism of action involved in the enhanced antitumor activity of CKAAKN-functionalized squalene-gemcitabine nanoparticles.

3. Conclusion

In a nutshell, we propose here a novel, efficient and easy method to prepare peptide-targeted squalene-based nanoparticles for pancreatic cancer treatment, able to specifically interact with both tumor cells and angiogenic vessels and capable of simultaneously promoting pericyte coverage, thus leading to the normalization of tumor blood vessels likely improving the tumor accessibility for the therapy. The superior efficacy of peptide-decorated nanoparticles compared with the non functionalized ones in RIP-Tag2 mice and our studies in pancreatic cancer cells suggest that the active targeting plays a key role in the improvement of the therapeutic efficacy of gemcitabine in experimental pancreatic cancers.

To our knowledge, this is the first successful example of pancreatic cancer targeted nanoparticles with unique selectivity and multiple mechanism of action.

Acknowledgments
The authors warmly thank Julie Mougin and Ghislaine Frébourg (Service of Electron Microscopy from IFR of Integrative Biology, Paris) for the cryo-TEM analysis and Dr. Valerie Nicolas (Service Imagerie-Microscopie Confocale, IFR-141 IPSIT, Châtenay-Malabry, France) for the expert assistance in confocal microscopy. The research leading to these results has received funding from the European Research Council under the European Community's Seventh Framework Programme FP7/2007-2013 Grant Agreement N°249835; from MIUR - University of Turin "Fondi Ricerca Locale (ex-60%)"; from Associazione Italiana per la Ricerca sul Cancro (AIRC) investigator grants IG (#11600); from Fondazione Piemontese per la Ricerca sul Cancro-Onlus (FPRC) (MIUR 5‰ E. Vaschetto, to E.G). F.M. was supported by "Post-doctoral Fellowships 2014" granted by Fondazione Umberto Veronesi (FUV). The authors acknowledge the Università Italo Francese/Université Franco Italienne for supporting the PhD co-tutoring of S.V.

Disclosure statement
The authors declare no competing financial interest.

Appendix A. Supplementary data
Supplementary data to this article can be found online at …

Figure captions

Fig. 1. Squalenoyl derivatives. Structure of dFdC **(1),** CKAAKN peptide **(4)** and their squalenoyl conjugates SQdFdC **(3)** and SQCKAAKN **(5)**.

Fig. 2. Characterization of SQdFdC and SQdFdC/SQCKAAKN NPs. Dynamic light scattering (DLS) data giving (a) **the average diameter in number** and (b) the zeta potential (ZP) of SQdFdC and SQdFdC/SQCKAAKN NPs. (c) Cryogenic transmission electron microscopy of SQdFdC/SQCKAAKN NPs. Scale bar: 100 nm.

Fig. 3. Surface plasmon resonance analysis of SQdFdC and SQdFdC/SQCKAAKN NPs. SPR sensorgrams (resonance units (RU) *versus* time) obtained by simultaneous injection of SQdFdC and SQdFdC/SQCKAAKN NPs (180 µM eq. SQ) over sFRP-4 immobilized on two parallel channels of the same sensor chip.

Fig. 4. Activation of C3 protein of the complement system. 2D electroimmunophoretic profile of complement activation for (a) SQdFdC NPs and (b) SQdFdC/SQCKAAKN NPs.

Fig. 5. Anti-tumor activity and apoptotic index. (a) Total tumor volume in a 2-weeks regression trial in RIP-Tag2 mice. Mice were injected intravenously (days 0, 3, 7 and 11) with either dFdC (15 mg/kg), SQdFdC NPs (15 mg/kg equiv. dFdC) or SQdFdC/SQCKAAKN NPs (15 mg/kg equiv. dFdC) (n=8/group). Tumor volume values **(86.08 mm^3, 45.97 mm^3, 31.01 mm^3 and 18.49 mm^3 for saline, dFdC, SQdFdC NPs and SQdFdC/SQCKAAKN NPs-treated mice, respectively),** represent means ± SD. Statistical difference is marked by **$p < 0.01$; ***$p < 0.001$). (b) Confocal analysis of five fields per mouse from each treatment

group immunostained with Meca32 (green) and cleaved caspase-3 (red). Apoptotic cancer cells are indicated with arrow heads and tumor vessels with arrows. Endothelial cells apoptotic rate was detected by colocalization of Meca32 (green) with activated caspase-3 (red). Scale bars: 50 μm. (c) Apoptotic index of cleaved caspase-3+ cells on total cells. Values represent mean ± SD. Statistical difference is marked by **p < 0.01.

Fig. 6. Immunohistochemical staining of tumor tissue-vessels and pericyte quantification. (a) Representative images (5 fields/mouse) of confocal analysis of Meca32 (green channel) endothelial marker immunostaining in tumor tissues from the different groups of treatment. Nuclei were stained with DAPI (blue channel). Scale bars: 50 μm. (b) Percentage of surface area occupied by vessels quantified as Meca32 positive staining. (c) Quantification analysis of **NG2** pericyte marker localized in proximity to endothelial cells-lined blood vessels. Values represent mean ± SD. Statistical difference is marked by **p < 0.01. (d) Tumor vessel pericyte coverage was evaluated as Meca32 (green channel) and **NG2** (red channel) colocalization. Images are representative of 5 fields per mouse from a total of 8 mice per treatment group. Scale bars: 50 μm.

Fig. 7. Representative images of confocal analysis of tumor sections after injection of fluorescently-labeled SQdFdC NPs or fluorescently-labeled SQdFdC/SQCKAAKN NPs (green channel).Tumor vessels were stained Meca32 (red channel) endothelial marker and nuclei with DAPI (blue channel). Free dye was used as negative control. Scale bars: 50 μm.

Fig. 8. Immunocytochemistry analysis and FZD-5 expression in tumor tissue. FZD-5 expression and localization in RIP-Tag2 tumors were assessed by immunofluorescence and confocal analysis. FZD-5 expressed on vessels is shown as co-staining of anti-FZD-5 antibody (red channel) with Meca32 (green channel). Nuclei were stained with DAPI (blue channel). The images shown are representative confocal microscopy of 5 fields per mouse. Scale bars: 50 μm.

Fig. 9. Schematic representation of the selective targeting of pancreatic tumor and multiple mechanism of action involved in the enhanced antitumor activity of CKAAKN-functionalized squalene-gemcitabine nanoparticles.

References

[1] A. Jemal, R. Siegel, J. Xu, E. Ward, Cancer statistics, 2010, CA Cancer J Clin, 60 (2010) 277-300.
[2] P.E. Oberstein, M.W. Saif, First-line treatment for advanced pancreatic cancer. Highlights from the "2011 ASCO Gastrointestinal Cancers Symposium". San Francisco, CA, USA. January 20-22, 2011, JOP, 12 (2011) 96-100.
[3] V. Heinemann, S. Boeck, A. Hinke, R. Labianca, C. Louvet, Meta-analysis of randomized trials: evaluation of benefit from gemcitabine-based combination chemotherapy applied in advanced pancreatic cancer, BMC Cancer, 8 (2008) 82.

[4] A. Sultana, C.T. Smith, D. Cunningham, N. Starling, J.P. Neoptolemos, P. Ghaneh, Meta-analyses of chemotherapy for locally advanced and metastatic pancreatic cancer, J Clin Oncol, 25 (2007) 2607-2615.
[5] M.J. Moore, D. Goldstein, J. Hamm, A. Figer, J.R. Hecht, S. Gallinger, H.J. Au, P. Murawa, D. Walde, R.A. Wolff, D. Campos, R. Lim, K. Ding, G. Clark, T. Voskoglou-Nomikos, M. Ptasynski, W. Parulekar, Erlotinib plus gemcitabine compared with gemcitabine alone in patients with advanced pancreatic cancer: a phase III trial of the National Cancer Institute of Canada Clinical Trials Group, J Clin Oncol, 25 (2007) 1960-1966.
[6] http://www.accessdata.fda.gov/drugsatfda_docs/appletter/2013/021660Orig1s037ltr.pdf, in.
[7] D.D. Von Hoff, T. Ervin, F.P. Arena, E.G. Chiorean, J. Infante, M. Moore, T. Seay, S.A. Tjulandin, W.W. Ma, M.N. Saleh, M. Harris, M. Reni, S. Dowden, D. Laheru, N. Bahary, R.K. Ramanathan, J. Tabernero, M. Hidalgo, D. Goldstein, E. Van Cutsem, X.Y. Wei, J. Iglesias, M.F. Renschler, Increased Survival in Pancreatic Cancer with nab-Paclitaxel plus Gemcitabine, New Engl J Med, 369 (2013) 1691-1703.
[8] L. Bildstein, C. Dubernet, V. Marsaud, H. Chacun, V. Nicolas, C. Gueutin, A. Sarasin, H. Benech, S. Lepetre-Mouelhi, D. Desmaele, P. Couvreur, Transmembrane diffusion of gemcitabine by a nanoparticulate squalenoyl prodrug: an original drug delivery pathway, J Control Release, 147 (2010) 163-170.
[9] K.P. Olive, M.A. Jacobetz, C.J. Davidson, A. Gopinathan, D. McIntyre, D. Honess, B. Madhu, M.A. Goldgraben, M.E. Caldwell, D. Allard, K.K. Frese, G. Denicola, C. Feig, C. Combs, S.P. Winter, H. Ireland-Zecchini, S. Reichelt, W.J. Howat, A. Chang, M. Dhara, L. Wang, F. Ruckert, R. Grutzmann, C. Pilarsky, K. Izeradjene, S.R. Hingorani, P. Huang, S.E. Davies, W. Plunkett, M. Egorin, R.H. Hruban, N. Whitebread, K. McGovern, J. Adams, C. Iacobuzio-Donahue, J. Griffiths, D.A. Tuveson, Inhibition of Hedgehog signaling enhances delivery of chemotherapy in a mouse model of pancreatic cancer, Science, 324 (2009) 1457-1461.
[10] Y. Takakura, R.I. Mahato, M. Hashida, Extravasation of macromolecules, Adv Drug Deliv Rev, 34 (1998) 93-108.
[11] D.E. Owens, 3rd, N.A. Peppas, Opsonization, biodistribution, and pharmacokinetics of polymeric nanoparticles, Int J Pharm, 307 (2006) 93-102.
[12] M. Hidalgo, Pancreatic cancer, N Engl J Med, 362 (2010) 1605-1617.
[13] J. Nicolas, S. Mura, D. Brambilla, N. Mackiewicz, P. Couvreur, Design, functionalization strategies and biomedical applications of targeted biodegradable/biocompatible polymer-based nanocarriers for drug delivery, Chem Soc Rev, 42 (2013) 1147-1235.
[14] S. Valetti, S. Mura, B. Stella, P. Couvreur, Rational design for multifunctional non-liposomal lipid-based nanocarriers for cancer management: theory to practice, Journal of Nanobiotechnology, 11 (2013) S6.
[15] J.W. Nichols, Y.H. Bae, Odyssey of a cancer nanoparticle: From injection site to site of action, Nano Today, 7 (2012) 606-618.
[16] R.A. Kudgus, A. Szabolcs, J.A. Khan, C.A. Walden, J.M. Reid, J.D. Robertson, R. Bhattacharya, P. Mukherjee, Inhibiting the growth of pancreatic adenocarcinoma in vitro and in vivo through targeted treatment with designer gold nanotherapeutics, PLoS One, 8 (2013) e57522.
[17] S. Ji, J. Xu, B. Zhang, W. Yao, W. Xu, W. Wu, Y. Xu, H. Wang, Q. Ni, H. Hou, X. Yu, RGD-conjugated albumin nanoparticles as a novel delivery vehicle in pancreatic cancer therapy, Cancer Biol Ther, 13 (2012) 206-215.
[18] E.R. Camp, C. Wang, E.C. Little, P.M. Watson, K.F. Pirollo, A. Rait, D.J. Cole, E.H. Chang, D.K. Watson, Transferrin receptor targeting nanomedicine delivering wild-type p53

gene sensitizes pancreatic cancer to gemcitabine therapy, Cancer Gene Ther, 20 (2013) 222-228.
[19] J. Xu, F. Gattacceca, M. Amiji, Biodistribution and pharmacokinetics of EGFR-targeted thiolated gelatin nanoparticles following systemic administration in pancreatic tumor-bearing mice, Mol Pharm, 10 (2013) 2031-2044.
[20] J.A. Joyce, P. Laakkonen, M. Bernasconi, G. Bergers, E. Ruoslahti, D. Hanahan, Stage-specific vascular markers revealed by phage display in a mouse model of pancreatic islet tumorigenesis, Cancer Cell., 4 (2003) 393-403.
[21] L.H. Reddy, P. Couvreur, Squalene: A natural triterpene for use in disease management and therapy, Adv Drug Deliv Rev, 61 (2009) 1412-1426.
[22] P. Couvreur, B. Stella, L.H. Reddy, H. Hillaireau, C. Dubernet, D. Desmaele, S. Lepetre-Mouelhi, F. Rocco, N. Dereuddre-Bosquet, P. Clayette, V. Rosilio, V. Marsaud, J.M. Renoir, L. Cattel, Squalenoyl nanomedicines as potential therapeutics, Nano Lett., 6 (2006) 2544-2548.
[23] D. Willner, P.A. Trail, S.J. Hofstead, H.D. King, S.J. Lasch, G.R. Braslawsky, R.S. Greenfield, T. Kaneko, R.A. Firestone, (6-Maleimidocaproyl)hydrazone of doxorubicin--a new derivative for the preparation of immunoconjugates of doxorubicin, Bioconjug Chem, 4 (1993) 521-527.
[24] H. Fessi, F. Puisieux, J.P. Devissaguet, N. Ammoury, S. Benita, Nanocapsule formation by interfacial polymer deposition following solvent displacement, International Journal of Pharmaceutics, 55 (1989) R1-R4.
[25] I. Bertholon, C. Vauthier, D. Labarre, Complement activation by core-shell poly(isobutylcyanoacrylate)-polysaccharide nanoparticles: influences of surface morphology, length, and type of polysaccharide, Pharm Res, 23 (2006) 1313-1323.
[26] G.H. M. Kazatchkine, U. Nydegger, , Techniques du complément, INSERM, Paris, (1986).
[27] C. Vauthier, B. Persson, P. Lindner, B. Cabane, Protein adsorption and complement activation for di-block copolymer nanoparticles, Biomaterials, 32 (2011) 1646-1656.
[28] D. Hanahan, Heritable formation of pancreatic beta-cell tumours in transgenic mice expressing recombinant insulin/simian virus 40 oncogenes, Nature, 315 (1985) 115-122.
[29] E. Giraudo, M. Inoue, D. Hanahan, An amino-bisphosphonate targets MMP-9-expressing macrophages and angiogenesis to impair cervical carcinogenesis, J Clin Invest, 114 (2004) 623-633.
[30] M. Zerlin, M.A. Julius, J. Kitajewski, Wnt/Frizzled signaling in angiogenesis, Angiogenesis, 11 (2008) 63-69.
[31] A.T. Weeraratna, Y. Jiang, G. Hostetter, K. Rosenblatt, P. Duray, M. Bittner, J.M. Trent, Wnt5a signaling directly affects cell motility and invasion of metastatic melanoma, Cancer Cell, 1 (2002) 279-288.
[32] D. Wawrzak, M. Metioui, E. Willems, M. Hendrickx, E. de Genst, L. Leyns, Wnt3a binds to several sFRPs in the nanomolar range, Biochem Biophys Res Commun, 357 (2007) 1119-1123.
[33] S.W. Reulen, P.Y. Dankers, P.H. Bomans, E.W. Meijer, M. Merkx, Collagen targeting using protein-functionalized micelles: the strength of multiple weak interactions, J Am Chem Soc, 131 (2009) 7304-7312.
[34] X. Montet, M. Funovics, K. Montet-Abou, R. Weissleder, L. Josephson, Multivalent effects of RGD peptides obtained by nanoparticle display, J Med Chem, 49 (2006) 6087-6093.
[35] J.D. Holland, A. Klaus, A.N. Garratt, W. Birchmeier, Wnt signaling in stem and cancer stem cells, Curr Opin Cell Biol, 25 (2013) 254-264.

[36] S. Schinner, H.S. Willenberg, M. Schott, W.A. Scherbaum, Pathophysiological aspects of Wnt-signaling in endocrine disease, Eur J Endocrinol, 160 (2009) 731-737.
[37] S. Yachida, S. Jones, I. Bozic, T. Antal, R. Leary, B.J. Fu, M. Kamiyama, R.H. Hruban, J.R. Eshleman, M.A. Nowak, V.E. Velculescu, K.W. Kinzler, B. Vogelstein, C.A. Iacobuzio-Donahue, Distant metastasis occurs late during the genetic evolution of pancreatic cancer, Nature, 467 (2010) 1114-U1126.
[38] P.J. Campbell, S. Yachida, L.J. Mudie, P.J. Stephens, E.D. Pleasance, L.A. Stebbings, L.A. Morsberger, C. Latimer, S. McLaren, M.L. Lin, D.J. McBride, I. Varela, S.A. Nik-Zainal, C. Leroy, M.M. Jia, A. Menzies, A.P. Butler, J.W. Teague, C.A. Griffin, J. Burton, H. Swerdlow, M.A. Quail, M.R. Stratton, C. Iacobuzio-Donahue, P.A. Futreal, The patterns and dynamics of genomic instability in metastatic pancreatic cancer, Nature, 467 (2010) 1109-1113.
[39] S. Jones, X. Zhang, D.W. Parsons, J.C. Lin, R.J. Leary, P. Angenendt, P. Mankoo, H. Carter, H. Kamiyama, A. Jimeno, S.M. Hong, B. Fu, M.T. Lin, E.S. Calhoun, M. Kamiyama, K. Walter, T. Nikolskaya, Y. Nikolsky, J. Hartigan, D.R. Smith, M. Hidalgo, S.D. Leach, A.P. Klein, E.M. Jaffee, M. Goggins, A. Maitra, C. Iacobuzio-Donahue, J.R. Eshleman, S.E. Kern, R.H. Hruban, R. Karchin, N. Papadopoulos, G. Parmigiani, B. Vogelstein, V.E. Velculescu, K.W. Kinzler, Core signaling pathways in human pancreatic cancers revealed by global genomic analyses, Science, 321 (2008) 1801-1806.
[40] V. Corbo, G. Tortora, A. Scarpa, Molecular Pathology of Pancreatic Cancer: From Bench-to-Bedside Translation, Current Drug Targets, 13 (2012) 744-752.
[41] J.P. Morris, S.C. Wang, M. Hebrok, KRAS, Hedgehog, Wnt and the twisted developmental biology of pancreatic ductal adenocarcinoma, Nat Rev Cancer, 10 (2010) 683-695.
[42] M. Katoh, WNT2 and human gastrointestinal cancer (review), Int J Mol Med, 12 (2003) 811-816.
[43] A.E. Nel, L. Madler, D. Velegol, T. Xia, E.M. Hoek, P. Somasundaran, F. Klaessig, V. Castranova, M. Thompson, Understanding biophysicochemical interactions at the nano-bio interface, Nat Mater, 8 (2009) 543-557.
[44] S.M. Moghimi, A.J. Andersen, S.H. Hashemi, B. Lettiero, D. Ahmadvand, A.C. Hunter, T.L. Andresen, I. Hamad, J. Szebeni, Complement activation cascade triggered by PEG-PL engineered nanomedicines and carbon nanotubes: the challenges ahead, J Control Release, 146 (2010) 175-181.
[45] S.M. Moghimi, Z.S. Farhangrazi, Nanomedicine and the complement paradigm, Nanomedicine, 9 (2013) 458-460.
[46] M.P. Carreno, F. Maillet, D. Labarre, M. Jozefowicz, M.D. Kazatchkine, Specific antibodies enhance Sephadex-induced activation of the alternative complement pathway in human serum, Biomaterials, 9 (1988) 514-518.
[47] C. Zandanel, C. Vauthier, Poly(isobutylcyanoacrylate) Nanoparticles Decorated with Chitosan: Effect of Conformation of Chitosan Chains at the Surface on Complement Activation Properties, Journal of Colloid Science and Biotechnology, 1 (2012) 68-81.
[48] G. Bergers, K. Javaherian, K.M. Lo, J. Folkman, D. Hanahan, Effects of angiogenesis inhibitors on multistage carcinogenesis in mice, Science, 284 (1999) 808-812.
[49] B.A. Teicher, Tumor models for efficacy determination, Mol Cancer Ther, 5 (2006) 2435-2443.
[50] G. Bergers, S. Song, N. Meyer-Morse, E. Bergsland, D. Hanahan, Benefits of targeting both pericytes and endothelial cells in the tumor vasculature with kinase inhibitors, J Clin Invest, 111 (2003) 1287-1295.
[51] F. Maione, F. Molla, C. Meda, R. Latini, L. Zentilin, M. Giacca, G. Seano, G. Serini, F. Bussolino, E. Giraudo, Semaphorin 3A is an endogenous angiogenesis inhibitor that blocks

tumor growth and normalizes tumor vasculature in transgenic mouse models, J Clin Invest, 119 (2009) 3356-3372.
[52] F. Maione, S. Capano, D. Regano, L. Zentilin, M. Giacca, O. Casanovas, F. Bussolino, G. Serini, E. Giraudo, Semaphorin 3A overcomes cancer hypoxia and metastatic dissemination induced by antiangiogenic treatment in mice, J Clin Invest, 122 (2012) 1832-1848.
[53] L.H. Reddy, C. Dubernet, S.L. Mouelhi, P.E. Marque, D. Desmaele, P. Couvreur, A new nanomedicine of gemcitabine displays enhanced anticancer activity in sensitive and resistant leukemia types, J Control Release, 124 (2007) 20-27.
[54] L.H. Reddy, J.M. Renoir, V. Marsaud, S. Lepetre-Mouelhi, D. Desmaele, P. Couvreur, Anticancer efficacy of squalenoyl gemcitabine nanomedicine on 60 human tumor cell panel and on experimental tumor, Mol Pharm, 6 (2009) 1526-1535.
[55] S. Rejiba, L.H. Reddy, C. Bigand, C. Parmentier, P. Couvreur, A. Hajri, Squalenoyl gemcitabine nanomedicine overcomes the low efficacy of gemcitabine therapy in pancreatic cancer, Nanomedicine, 7 (2011) 841-849.
[56] R.K. Jain, Normalization of tumor vasculature: an emerging concept in antiangiogenic therapy, Science, 307 (2005) 58-62.